

Research Paper

Diagnosis of newly developed multiple myeloma without bone disease detectable on conventional computed tomography (CT) scan by using dual-energy CT

Nan Jiang^{b,1}, Yu Xia^{b,1}, Mingcong Luo^{b,1}, Jianhua Chen^b, Zongjian Qiu^c, Jianfang Liu^{a,b,*}

^a Department of Radiology, The First Affiliated Hospital of Xiamen University, School of Medicine, Xiamen University, Xiamen, China

^b Department of Radiology, Fujian Medical University Union Hospital, 29 Xin Quan Road, Gulou District, Fuzhou, Fujian 350001, China

^c Fujian Institute of Hematology, Fujian Provincial Key Laboratory on Hematology, Fujian Medical University Union Hospital, Fuzhou, Fujian 350001, China

HIGHLIGHTS

- DECT could help detecting multiple myeloma without bone disease.
- Grouping and analyzing spinal segments can enhance diagnostic results.
- For middle-lower thoracic, $D_{\text{Fat(HAP)}}$ got 78.1 % accuracy with a cut-off of 955 mg/cm³.
- For thoracolumbar, $D_{\text{Fat(HAP)}}$ got 77.1 % accuracy with a cut-off of 947 mg/cm³.
- For middle-lower lumbar, $D_{\text{Fat(HAP)}}$ got 81.6 % accuracy with a cut-off of 947 mg/cm³.

ARTICLE INFO

Keywords:

Multiple myeloma
Dual energy
Computed tomography
Bone disease
Bone marrow

ABSTRACT

Objective: To evaluate the diagnostic utility of fat (hydroxyapatite) density [$D_{\text{Fat (HAP)}}$] on dual-energy computed tomography (DECT) for identifying clinical diagnosed multiple myeloma without bone disease (MNBD) that is not visible on conventional CT scans.

Material and Methods: In this age-gender-examination sites matched case control prospective study, Chest and/or abdominal images on Revolution CT of MNBDs and control subjects were consecutive enrolled in a 1:2 ratio from October 2022 to November 2023. Multiple myeloma was clinical diagnosed according to criteria of the International Myeloma Working Group. Regions of interest (ROIs) were drawn separately for all thoracolumbar vertebrae in the scanning range by two radiologists. Additionally, a radiologist specializing in musculoskeletal imaging supervised the process. $D_{\text{Fat (HAP)}}$ was extracted from each ROI. The spine was divided into upper thoracic (UPT), middle and lower thoracic (MLT), thoracolumbar (TL), and middle and lower lumbar (MLL) vertebrae. The area under the receiver operating characteristic curve (AUC) was calculated to evaluate the diagnostic performance of $D_{\text{Fat (HAP)}}$ in diagnosing multiple myeloma, and the sensitivity, specificity, and accuracy under the optimal cut-off were determined by Youden index (sensitivity + specificity - 1).

Results: A total of 32 and MNBD patients and 64 control patients were included. The total number of ROIs outlined included MNBD group (n = 493) and control group (n = 986). For all vertebrae, $D_{\text{Fat(HAP)}}$ got average performance in the diagnosis of MNBD (AUC = 0.733, $p < 0.001$) with a cut-off value of 958 (mg/cm³); the sensitivity, specificity, and accuracy were 58.8 %, 77.8 %, and 71.7 %, respectively. Regarding segment analysis, the diagnostic performance was good for all (AUC, 0.803–0.837; $p < 0.001$) but the UPT segment (AUC = 0.692, $p = 0.002$). The optimal diagnostic cut-off values for the MLT, TL, and MLL vertebrae were 955 mg/cm³, 947 mg/cm³, and 947 mg/cm³, respectively; the sensitivity, specificity, and accuracy were 80.0 %-87.5 %, 71.9 %-82.6 %, and 77.1 %-81.6 %, respectively.

Conclusion: DECT was effective for detecting MNBD, and better diagnostic results can be obtained by grouping different spine segments.

* Corresponding author at: Department of Radiology, The first affiliated Hospital of Xiamen University, 55 Zhen Hai Road, Siming District. Xiamen, Fujian 361000, China.

E-mail address: liujianfang1210@163.com (J. Liu).

¹ Nan Jiang, Yu Xia, and Mingcong Luo have contributed equally to this work and share first authorship.

Abbreviation

MM	multiple myeloma
MNBD	multiple myeloma with no bone disease
DECT	dual-energy CT
$D_{\text{Fat(HAP)}}$	fat (hydroxyapatite) density
MDE	myeloma defining events
UPT	upper thoracic vertebrae
MLT	middle and lower thoracic vertebrae
TL	thoracolumbar vertebrae
MLL	middle and lower lumbar vertebrae
ROC	receiver operating characteristic
AUC	area under the ROC curve
YI	Youden index

1. Introduction

Multiple myeloma (MM) is the second most common hematological tumor and among the most difficult malignancies to diagnose [1,2]. Bone pain is the most common MM symptom, with over 50 % of patients experiencing bone pain, particularly chest and back pain. However, the median time from the initial recording of bone pain to MM diagnosis has been reported to be 220 days [3]. Diagnostic delays adversely affect clinical processes and outcomes [4]. Therefore, early MM diagnosis is important. However, a sensitive, specific, and economical MM screening method is lacking [5].

Computed tomography (CT) has a high sensitivity for diagnosing osteolytic lesions, making it the preferred imaging modality for MM diagnosis [6–8]. The International Multiple Myeloma Working Group defines MM-associated bone disease (MBD) as the detection of more than one osteolytic lesion on CT, radiography, or positron emission tomography CT [9–11]. However, only when plasma cells infiltrate to a certain extent can MBD occur. Therefore, there are still some patients who show as osteoporosis, osteopenia, or no significant bone abnormality detectable on conventional CT, we defined those patients as MM with no obvious bone disease (MNBD). Conventional CT lacks specificity for evaluating osteoporosis or osteopenia, making distinguishing between MM and osteoporosis or osteopenia in middle-aged or elderly individuals difficult [12]. Furthermore, conventional CT has a high false-negative rate in patients with diffuse infiltration of bone marrow stromal cells and no trabecular or cortical bone destruction [13]. Therefore, the diagnostic value of conventional CT for MNBD is limited.

Magnetic resonance imaging (MRI) is among the most sensitive imaging modalities for detecting MM-related bone marrow abnormalities; however, its long acquisition time, high cost, and many contraindications have affected its widespread application. Dual-energy CT (DECT) can enable separation of bone trabeculae and bone marrow through material separation technology. DECT is suitable for patients who can't undergo MRI and can effectively diagnose bone marrow infiltration in MM [14–18]. DECT is valuable for evaluating trauma, vertebral compression fractures, and osteoporosis [19]. Moreover, with the advancement of DECT scanner technology, the radiation dose has been significantly reduced. Consequently, the additional radiation burden is considered acceptable, particularly in elderly patients.

However, there are still few specialized reports on the use of DECT for diagnosing MNBD. Furthermore, the CT Hounsfield unit (HU) of normal vertebrae has been reported to reduce with progression in the craniocaudal direction [20]. Vertebrae infiltrated by MM plasma cells have a more uniform tissue structure as infiltration increases [21]. Further research is needed to determine whether the diagnostic performance of DECT can be changed by the position of vertebral segments. Therefore, this study aimed to evaluate the diagnostic utility of fat (hydroxyapatite) density [$D_{\text{Fat (HAP)}}$] on DECT for identifying clinical

diagnosed MNBD that is not visible on conventional CT scans.

2. Materials and methods

2.1. Patient selection

This study was conducted according to the tenets of the Declaration of Helsinki (as revised in 2013). The single-center study was approved by our hospital's ethics committee and informed consent was obtained from all participants.

This was a prospective age-gender-examination sites matched case control study, with MNBDs and control subjects consecutive included in a 1:2 ratio from October 2022 to November 2023. The inclusion criteria were as follows: (1) the MNBDs group will include individuals who were newly diagnosed with or suspected of having MM. (2) the control group will include non-MM individuals who had a history of back pain and/or low back pain, and underwent chest and/or abdominal CT per the recommendation of the attending physician. The exclusion criteria were as follows: (1) MM with MBD detectable on standard CT scan; (2) metabolic and hematopoietic diseases other than osteoporosis; (3) other oncological or autoimmune diseases; (4) spinal trauma or postoperative of the vertebral and (5) severe image artifacts.

2.2. Clinical diagnosis of MM

According to criteria of the International Myeloma Working Group: the diagnosis requires ≥ 10 % clonal bone marrow plasma cells or a biopsy-proven plasmacytoma plus evidence of one or more multiple myeloma defining events (MDE): hypercalcemia, renal failure, anemia, or lytic bone lesions attributable to the plasma cell disorder, bone marrow clonal plasmacytosis ≥ 60 %, serum involved/uninvolved free light chain (FLC) ratio ≥ 100 (provided involved FLC is ≥ 100 mg/L), or > 1 focal lesion on magnetic resonance imaging [11].

2.3. DECT protocol

The Revolution CT scanner (GE Healthcare, Waukesha, WI, USA) was used to perform non-enhanced chest and/or abdominal DECT. The parameters were as follows: rapid switching of 80–140 kV tube voltage; automatic mA modulation technology; pitch, 1.375; collimation width, 40 mm; matrix, 512 \times 512; scanning layer thickness, 1.25 mm; and layer spacing, 0.625 mm. The scanner was calibrated before the study, and scans were performed daily during the study period to assess quality and confirm unchanged scanner performance.

2.4. Data post-processing

The GSI viewer on the AW4.7 workstation (GE Healthcare) was used to analyze DECT data files. This software can reconstruct 70 keV monochromatic images and fat (HAP) images (i.e., virtual removal of HAP images) and obtain corresponding CT values (HU) and fat (HAP) material density values [$D_{\text{Fat (HAP)}}$] (mg/cm^3) by outlining regions of interest (ROIs). The CT numbers on the 70 keV monochromatic images were measured because the conventional polychromatic images at 120 kVp had an average energy of approximately 70 keV in GSI mode [22].

2.5. ROI delineation

ROIs were drawn separately for all thoracolumbar vertebrae in the scanning range. They were delineated by two radiologists with 3 years of experience in musculoskeletal imaging (Reader 1 and Reader 2). Another radiologist with 9 years of experience in musculoskeletal imaging (Reader 3) supervised the process. The principle of ROI delineation is to select the maximum level of the vertebral body on the reconstructed sagittal 70 keV monochromatic images and avoid the intervertebral foramen, cortical bone, bone islands, Schmorl nodules,

and hemangiomas (Fig. 1). At the same time, the GSI viewer software matched ROIs to the fat (HAP) images.

The spine was divided into four segments according to the anatomical and weight-bearing characteristics of the vertebrae: upper thoracic (UPT) (T1-T4), middle and lower thoracic (MLT, T5-T10), thoracolumbar (TL, T11-L1), and middle and lower lumbar (MLL; L2-5) vertebrae. The CT value and $D_{\text{Fat (HAP)}}$ of each spine segment are the mean values of the vertical that make up each spine segment.

2.6. Statistical analysis

SPSS 26.0 (IBM Corp., Armonk, NY, USA) was used for statistical analysis. $P < 0.05$ was considered significant. Intraobserver agreements were evaluated by calculating the intraclass correlation coefficients. The t -test or Mann-Whitney U test was used to compare continuous variables, and the chi-square test was used to compare categorical variables. For multiple-group comparisons, the variance analysis was used, and the least significant difference (LSD) method was used for correction. Receiver operating characteristic curve (ROC), the most commonly used tool in diagnostic research, is a graphical summary of the discriminative capacity of a thresholded continuous scoring system for a binary outcome [23]. The curve consists of pairs of sensitivity and specificity as the threshold is varied. As a rule of thumb, the threshold with the largest Youden index, which equals to sensitivity + specificity - 1, was the optimal cutoff point value [24]. Parameter (CT values or $[D_{\text{Fat (HAP)}]}$) greater than optimal cut-off values as the best discriminating value associated with MNBDs, and corresponding accuracy can be calculated using standard equations. The area under the curve (AUC) was calculated to compare the diagnostic performances. According to the AUC value, the diagnostic performance was classified as fail (0.5–0.6), poor (0.6–0.7), average (0.7–0.8), good (0.8–0.9), and great (0.9–1.0) [25].

3. Results

From October 2022 to November 2023, 95 MM and 90 control consecutive patients were conducted DECT in our institute. The flow-chart of patient inclusion in this study is shown in Fig. 2. And a total of 32 MNBD patients (mean age, 59.3 ± 13.9) and 64 control patients (mean age, 60.9 ± 12.9) were finally included in this study. There was no statistical difference in sex composition and age between the MNBD and control groups (Table 1). All these 96 patients underwent chest DECT examinations, including 25 MNBDs and 50 control patients not only underwent chest DECT but also abdominal DECT. The total number of ROIs outlined included MNBD group ($n = 493$) and control group (n

$= 986$). The number of vertebral bodies in each spine segment is shown in Table 1.

3.1. Intraclass correlation coefficient analyses

The quantitative parameters measured by Reader 1 and Reader 2 had excellent consistency, and the intraclass correlation coefficient was 0.936.

3.2. Comparison of CT values and $D_{\text{Fat (HAP)}}$ between the MNBD and control group

For all vertebrae, the CT values of the MNBD group were lower than those of the control group (181.4 ± 72.9 vs. 203.2 ± 76.3 , $p < 0.001$), and the $D_{\text{Fat (HAP)}}$ of the MNBD group was higher than that of the control group (960.0 ± 16.3 vs. 948.2 ± 17.8 , $p < 0.001$) (Table 2).

There was no evidence of differences in CT values for any of the four spine segments between the MNBD and control groups ($p \geq 0.05$). For any of the four spine segments, the $D_{\text{Fat (HAP)}}$ for the MNBD group was higher than that for the control group ($p < 0.001$) (Table 2).

3.3. Comparison of CT values and $D_{\text{Fat (HAP)}}$ of the different spine segments

Regarding the MNBD group, except for the CT values of UPT being higher than those of MLT ($p < 0.05$), there was no evidence of a difference in CT values and $D_{\text{Fat (HAP)}}$ among the other spine segments ($p \geq 0.05$) (Table 2 and Fig. 3).

For the control group, the CT value and $D_{\text{Fat (HAP)}}$ of the upper spine segments were higher than the corresponding values for the lower spine segments ($p < 0.05$) (Table 2 and Fig. 3).

3.4. Performance of the CT value and $D_{\text{Fat (HAP)}}$ in diagnosing MNBDs

(1) Regarding the vertebral analysis:

CT values failed to diagnose MNBDs ($\text{AUC} = 0.427$, $p < 0.001$), the optimal cutoff value for CT value to diagnose MNBDs was $155(\text{mg}/\text{cm}^3)$. And when using CT value $> 155(\text{mg}/\text{cm}^3)$ as a criterion to diagnose MNBDs, the YI, sensitivity, specificity, and accuracy were -0.121 , 60.3 %, 27.5 %, and 38.1 %, respectively.

$D_{\text{Fat(HAP)}}$ got average performance in the diagnosis of MNBDs ($\text{AUC} = 0.733$, $p < 0.001$), the optimal cutoff value for $D_{\text{Fat(HAP)}}$ to diagnose MNBDs was $958(\text{mg}/\text{cm}^3)$. And when using $D_{\text{Fat(HAP)}} > 958(\text{mg}/\text{cm}^3)$ as a criterion to diagnose MNBDs, the YI, sensitivity, specificity, and

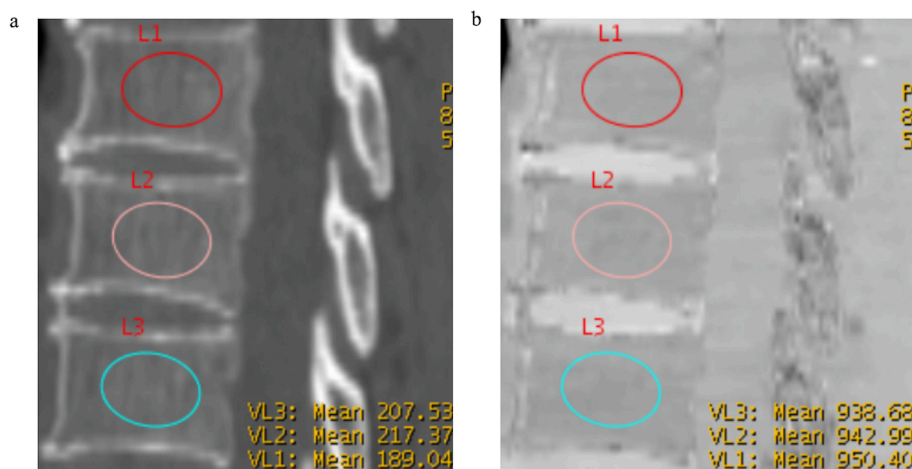


Fig. 1. Sketch map of regions of interest. a. 70 keV monoenergetic CT imaging; b. Fat (HAP) imaging. The principle of ROI delineation is to select the maximum level of the vertebral body on the reconstructed sagittal 70 keV monochromatic images and avoiding intervertebral foramen, cortical bone, bone islands, Schmorl nodules, and hemangiomas. At the same time, the GSI viewer software was used to match ROIs to fat (HAP) images.

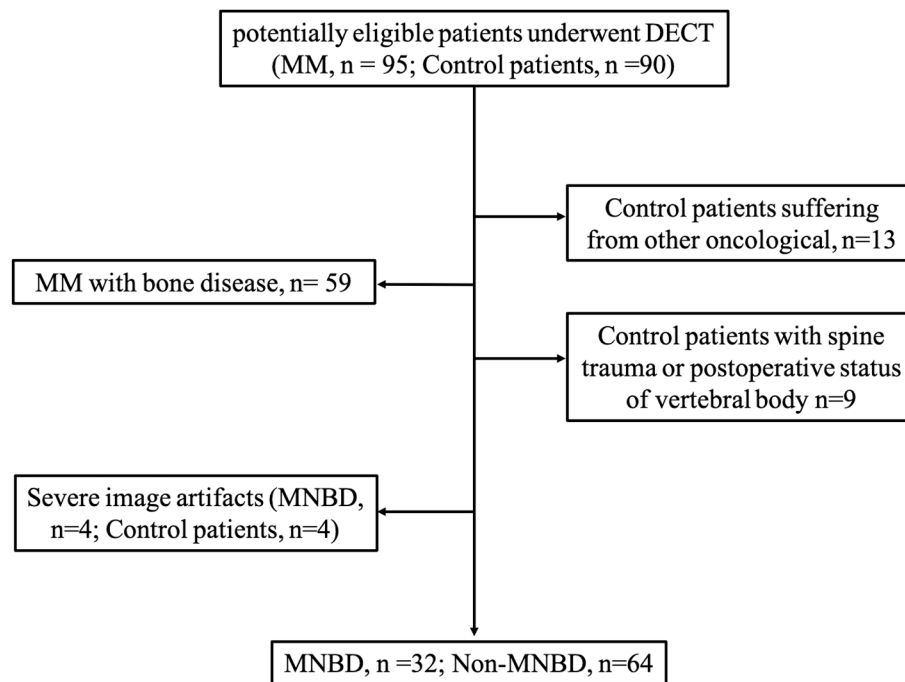


Fig. 2. Patient selection flow chart. DECT, dual-energy CT; MM, multiple myeloma; MNBD, multiple myeloma without bone disease.

Table 1
Basic clinical characteristics of the study population.

Variable	MNBD group (n = 32)	Control group (n = 64)	p
Age (years)	59.3 ± 13.9	60.9 ± 12.9	0.56
Sex (n)			
Male	15 (46.9 %)	32 (50 %)	0.77
Female	17 (53.1 %)	32 (50 %)	
Segment (n)			
UPT	32	64	
MLT	32	64	
TL	32	64	
MLL	25	51	

MNBD, multiple myeloma without bone disease; UPT, upper thoracic vertebrae; MLT, middle and lower thoracic vertebrae; TL, thoracolumbar vertebrae; MLL, middle and lower lumbar vertebrae.

accuracy were 0.366, 58.8 %, 77.8 %, and 71.7 %, respectively. (Table 3, Fig. 4).

(2) Regarding the spine segment analysis:

CT values still make failure performance in diagnosing MNBDs (AUC = 0.429–0.531, $p = 0.260$ – 0.698). When the $D_{\text{Fat(HAP)}}$ value was used as the diagnostic criterion for MNBD, the diagnostic performance was good for all (AUC, 0.803–0.837; $p < 0.001$) but the UPT segment (AUC = 0.692, $p = 0.002$) (Table 3 and Fig. 4).

The optimal diagnostic cutoff of $D_{\text{Fat(HAP)}}$ for the UPT, MLT, TL, and MLL vertebrae were 960 mg/cm³, 955 mg/cm³, 947 mg/cm³, and 947 mg/cm³, respectively. For the UPT segment, the YI, sensitivity, specificity, and accuracy were 0.375, 59.4 %, 78.1 %, and 71.9 %, respectively. The corresponding values for the MLT, TL, and MLL segments were 0.578–0.624, 80.0 %-87.5 %, 71.9 %-82.6 %, and 77.1 %-81.6 % (Table 3).

4. Discussion

In this study, we investigated the efficiency of $D_{\text{Fat(HAP)}}$ acquired from DECT in detecting MNBD. We found that the CT value and $D_{\text{Fat(HAP)}}$ of MNBD were not significantly different among most vertebral segments of the control group, while the CT value and $D_{\text{Fat(HAP)}}$ of the upper

Table 2
Comparison of CT values and $D_{\text{Fat(HAP)}}$ for different spine segments between the MNBD and control groups.

Spine	CT values (HU)			$D_{\text{Fat(HAP)}}$ (mg/cm ³)		
	MNBD group	Control group	p	MNBD group	Control group	p
ALL	181.4 ± 72.9	203.2 ± 76.3	0<.001	960.0 ± 16.3	948.2 ± 17.8	< 0.001
UPT	198.6 ± 69.5	217.4 ± 66.3	0.20	960.8 ± 15.3	951.7 ± 13.1	< 0.001
MLT	175.55 ± 66.3	182.7 ± 63.6	0.61	961.6 ± 16.1	948.1 ± 9.6	< 0.001
TL	173.4 ± 68.2	169.3 ± 62.9	0.77	958.1 ± 15.0	942.0 ± 9.9	< 0.001
MLL	162.1 ± 69.7	160.6 ± 64.2	0.93	955.4 ± 15.1	936.9 ± 11.8	< 0.001

MNBD, multiple myeloma without bone disease; $D_{\text{Fat(HAP)}}$, Fat(HAP) density; ALL, all vertebrae; UPT, upper thoracic, MLT, middle and lower thoracic; TL, thoracolumbar; MLL, middle and lower lumbar.

spine segment of the control group are higher than those of the lower spine segment. Our findings suggest that $D_{\text{Fat(HAP)}}$ determined using DECT can diagnose MNBD effectively, and better diagnostic results can be obtained by grouping and analyzing different spine segments.

Either osteolytic lesions detected by CT, PET/CT or skeletal radiography, or focal lesions diagnosed by MRI are MDE [26]. CT is the best method for evaluating osteolytic lesions in MM. Considering osteoporosis and compression fractures alone as criteria for MDE could result in over diagnosing multiple myeloma in elderly patients. The International Myeloma Working Group states that osteoporosis or vertebral compression fractures without lytic lesions are no longer adequate for diagnosing bone disease in multiple myeloma [26]. However, patients with osteoporosis, osteopenia, or normal bone CT scans can still have MM, which were the MNBD patients we studied. Although MM typically affects middle-aged and elderly individuals, it can also occur in younger patients. In younger patients with monoclonal gammopathy who have vertebral compression fractures, further imaging like CT or PET-CT is needed to rule out myeloma. But it should be noted that, in these younger patients, their dense vertebral bodies may make osteopenia

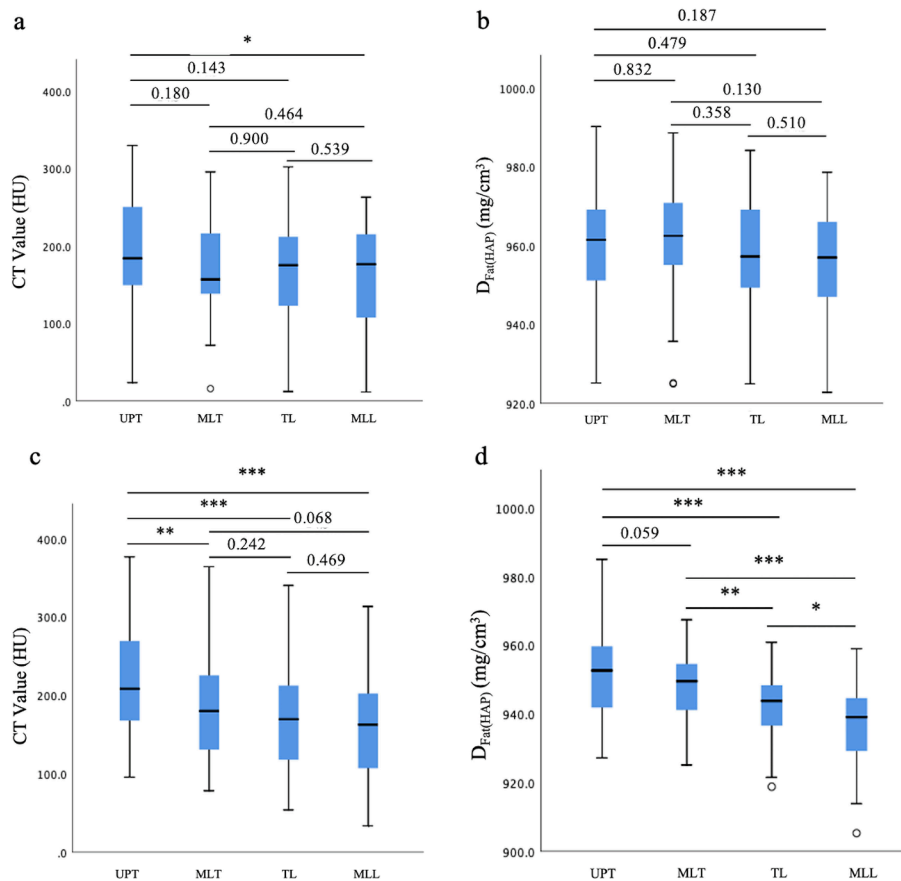


Fig. 3. Comparison of CT values and $D_{Fat(HAP)}$ across different spine segments. a. Comparison of CT values of different spinal segments in MNBD group. b. Comparison of $D_{Fat(HAP)}$ of different spinal segments in MNBD group; c. Comparison of CT values of different spinal segments in control group; d. Comparison of $D_{Fat(HAP)}$ of different spinal segments in control group. $*0.01 < P < 0.05$; $**0.01 < P < 0.001$; $***0.001 < P < 0.0001$. Groups were compared pairwise by using post hoc t-tests based on data from all groups and one-way ANOVA.

Table 3

Diagnostic performance of CT value and $D_{Fat(HAP)}$ in differentiating MNBDs from control patients across different spine segments.

Parameter	AUC (95 % CI)	YI	Cut off	Sen (%)	Spe (%)	Acc (%)
ALL CT value	0.427 (0.296, 0.458)	-0.121	155	60.3	27.5	38.1
ALL $D_{Fat(HAP)}$	0.733 (0.704, 0.761)	0.366	958	58.8	77.8	71.7
UPT CT value	0.429 (0.306, 0.553)	0.234	187	56.3	67.2	63.5
UPT $D_{Fat(HAP)}$	0.692 (0.576, 0.808)	0.375	960	59.4	78.1	71.9
MLT CT value	0.476 (0.351, 0.601)	-0.094	151	59.4	31.3	40.6
MLT $D_{Fat(HAP)}$	0.803 (0.691, 0.914)	0.578	955	81.3	76.6	78.1
TL CT value	0.531 (0.405, 0.657)	0.125	196	43.8	68.8	60.4
TL $D_{Fat(HAP)}$	0.830 (0.730, 0.929)	0.594	947	87.5	71.9	77.1
MLL CT value	0.521 (0.377, 0.665)	0.167	174	52.0	64.7	60.5
MLL $D_{Fat(HAP)}$	0.837 (0.732, 0.942)	0.624	947	80.0	82.4	81.6

MNBD, multiple myeloma with no bone disease; $D_{Fat(HAP)}$, Fat(HAP) density; ALL, all vertebrae; UPT, upper thoracic; MLT, middle and lower thoracic; TL, thoracolumbar; MLL, middle and lower lumbar; AUC, area under the ROC curve; YI, Youden index; Sen, sensitivity; Spe, specificity; Acc, accuracy.

harder to detect, complicating MM diagnosis. MRI, a noninvasive alternative methods for diagnosis bone marrow infiltration especially in young patients, is the most effective imaging modality for assessing focal bone marrow lesions before true osteolytic disease occurs [27]. MRI may show focal lesions (MDE) in MNBD patients, aiding in MM diagnosis. However, besides the two patterns of focal and combined diffuse-focal infiltration, there are three modes: diffuse infiltration pattern, salt-and-pepper infiltration pattern, and the normal pattern [28]. And in addition to the normal pattern, diffuse pattern has also not yet been considered a member of MDE by the International Myeloma Working Group [9]. Hu C et al. propose that the analysis of DECT holds promise as a quantitative method for detecting bone marrow infiltration and assessing infiltration patterns in MM patients[18]. The findings of Chen et al. suggest that DECT may effectively differentiates MM patients with diffuse pattern from controls (non-MM) and shows moderate accuracy in distinguishing normal pattern MM from non-MM [29]. Therefore, in this DECT study, the reference standard for the diagnosis of multiple myeloma (MM) is based on clinical diagnosis according to criteria of the International Myeloma Working Group rather than on bone marrow infiltration as determined by MRI.

DECT is used in musculoskeletal imaging for the detection of crystal arthropathy and subtle fracture detection; however, it is not widely used in the evaluation of invasive skeletal lesions [19]. Previous studies have shown that DECT does not have improved detection efficiency for osteolytic lesions [14]. In this study, we concentrated on MNBD, a condition that poses diagnostic challenges with conventional CT imaging. We use DECT to diagnose MNBD and achieved good performance. Previous studies on DECT evaluation of MNBD have achieved promising

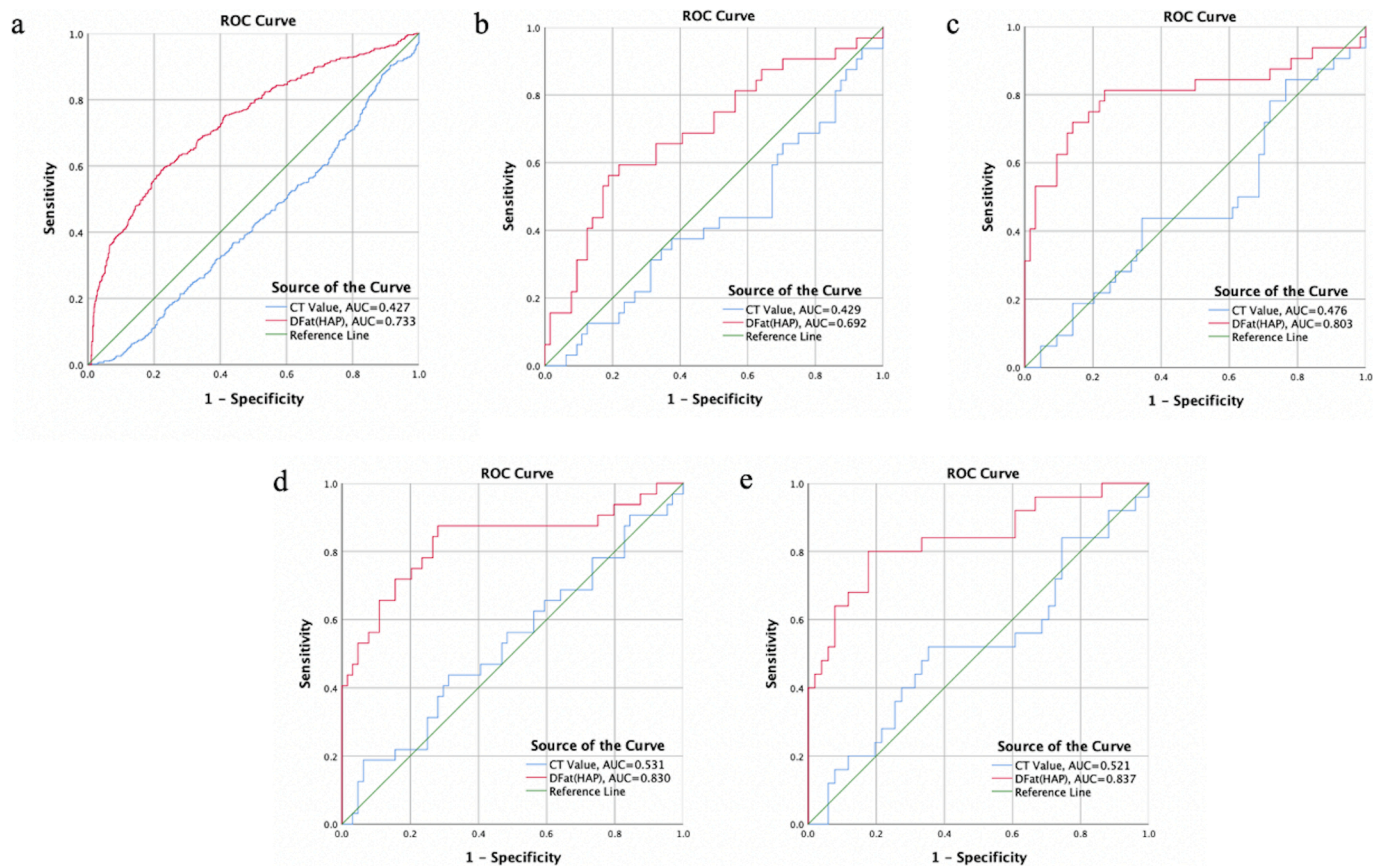


Fig. 4. Performance of CT value and $D_{\text{Fat}}(\text{HAP})$ in distinguishing MNBDs from control patients. a. ROC curves for all vertebrae; b. ROC curves for upper thoracic vertebrae, c. ROC curves for middle and lower thoracic vertebrae; d. ROC curves for thoracolumbar vertebrae; e. ROC curves for middle and lower lumbar vertebrae.

results; however, they were based on the analyses of small samples. For example, in the studies by Thomas et al. and Fervers et al. involving the use of dual-source DECT for virtual non-calcium imaging of MM, only 10 and 8 cases MNBD, respectively, were included [14; 17]. The present study differs from previous ones: First, this study included preliminary screening of MM, thus previously treated patients with MM were excluded and only those newly diagnosed with MM were included. DECT image acquisition techniques from different manufacturers may vary. Most previous studies on MM were based on the three-material decomposition technique of dual-source DECT, obtaining virtual non-calcium images [30]. Chen et al. found that the two-material decomposition technique in rapid voltage switching DECT, which eliminates the X-ray absorption components of HAP, is effective for the diagnosis of non-osteolytic MM in the spine, regardless of the paired material [29]. In this study the images are generated from two basic paired materials (Fat-HAP) based on their respective atomic numbers and mass-attenuation coefficients. Our study suggests that two-material decomposition based on rapid voltage switching DECT can help detect MNBD well via the determination of $D_{\text{Fat}}(\text{HAP})$.

Schröder et al. investigated the vertebrae of human cadavers and found that the failure load and endplate sizes of normal vertebrae increased progressively in the cranio-caudal direction, while the CT value reduced [20]. This is consistent with our results, which show that the CT value and $D_{\text{Fat}}(\text{HAP})$ of the normal vertebral body vary according to the segment of the spine, and the CT value and $D_{\text{Fat}}(\text{HAP})$ of the upper spine segment were higher than those of the lower spine segment. In addition, our study showed that for MNBD, CT values and $D_{\text{Fat}}(\text{HAP})$ were not significantly different among most vertebral segments. Reinert et al also pointed out that with increased medulla infiltration, the tissue structure of MM became more uniform and attenuation was higher [21]. This is likely because the normal composition of the vertebral body is

more affected by the weight-bearing on the vertebral body, while physiologic difference of bone density for each spinal segment in MM patients is obscured due to infiltration of the disease. Therefore, compared to MNBD, the CT values and $D_{\text{Fat}}(\text{HAP})$ of normal vertebrae are more susceptible to the influence of spine segments.

Previous DECT studies on MNBD often randomly selected vertebral bodies for analysis [14–16;18]. Due to the varying degrees of influence of spinal segments on the vertebral body composition of MNBDs and control patients, we conducted a grouping analysis of different vertebral segments. We found that the diagnostic performance was good for all but the UPT segment. The optimal cut-off values for UPT and MLT vertebrae were similar (960 mg/cm^3 vs. 955 mg/cm^3), and the optimal diagnostic cutoff value for both the TL and MLL segments was 947 mg/cm^3 . Perhaps it is because the composition of the bone in the UPT and MLT segments is similar, while that of the TL and MLL is similar. The UPT spine segment is close to the thoracic entrance and is easily affected by the hardening artifacts at the thoracic entrance, which may be the reason for its poor diagnostic performance. Therefore, we suggest that the utility of $D_{\text{Fat}}(\text{HAP})$ for diagnosing MNBD should be analyzed in segments, and it is not recommended to use UPT spine segments for analysis. For the MLT segments, the diagnostic criteria for MNBD should be $D_{\text{Fat}}(\text{HAP}) \geq 960 \text{ mg/cm}^3$, and for the TL and lumbar segments, the diagnostic criteria for MNBD should be $D_{\text{Fat}}(\text{HAP}) \geq 947 \text{ mg/cm}^3$.

Our study has some limitations. This study was a pilot study and did not include an analysis of the cervical and sacrococcygeal vertebrae. Further research is needed in the future. Furthermore, owing to device limitations, we did not compare the diagnostic performance of rapid voltage switching DECT $D_{\text{Fat}}(\text{HAP})$ images with dual-source DECT virtual non-calcium images.

In conclusion, our study suggests that DECT is an effective detection method for MNBD, and better diagnostic results can be obtained by

grouping different spine segments.

CRedit authorship contribution statement

Nan Jiang: Writing – original draft, Methodology, Investigation, Formal analysis. **Yu Xia:** Writing – original draft, Software, Investigation, Formal analysis. **Mingcong Luo:** Writing – original draft, Software, Methodology, Formal analysis. **Jianhua Chen:** Supervision, Data curation. **Zongjian Qiu:** Supervision, Resources. **Jianfang Liu:** Writing – review & editing, Supervision, Project administration, Funding acquisition.

Declaration of competing interest

The authors declare that they have no known competing financial interests or personal relationships that could have appeared to influence the work reported in this paper.

Acknowledgements

This research was supported by Natural Science Foundation of Fujian Province (Youth Innovation) (Grant No. 2023 J05040).

Appendix A. Supplementary data

Supplementary data to this article can be found online at <https://doi.org/10.1016/j.jbo.2024.100636>.

References

- [1] J. Liu, W. Liu, L. Mi, et al., Incidence and mortality of multiple myeloma in China, 2006–2016: an analysis of the Global Burden of Disease Study 2016, *J. Hematol. Oncol.* 12 (2019) 136, <https://doi.org/10.1186/s13045-019-0807-5>.
- [2] D.A. Howell, A.G. Smith, A. Jack, et al., Time-to-diagnosis and symptoms of myeloma, lymphomas and leukaemias: a report from the Haematological Malignancy Research Network, *BMC Hematol* 13 (2013) 9, <https://doi.org/10.1186/2052-1839-13-9>.
- [3] A. Seesagur, N. Petruski-Ivleva, V.L. Banks, et al., Clinical features and diagnosis of multiple myeloma: a population-based cohort study in primary care, *BMJ Open* 11 (2021) e052759.
- [4] J. Carmichael, F. Seymour, G. McLroy, et al., Delayed diagnosis resulting in increased disease burden in multiple myeloma: the legacy of the COVID-19 pandemic, *Blood Cancer J.* 13 (2023) 38, <https://doi.org/10.1038/s41408-023-00795-w>.
- [5] M. Morawska, J. Dwilewicz-Trojaczek, T. Stompór, et al., A Stepwise Screening Protocol for Multiple Myeloma, *J. Clin. Med.* 8;12(4):1345 (2023), <https://doi.org/10.3390/jcm12041345>.
- [6] M.T. Winkelmann, F. Hagen, L. Le-Yannou, et al., Myeloma bone disease imaging on a 1st-generation clinical photon-counting detector CT vs. 2nd-generation dual-source dual-energy CT, *Eur. Radiol.* 33 (2023) 2415–2425, <https://doi.org/10.1007/s00330-022-09225-0>.
- [7] J. Hillengass, S. Usmani, S.V. Rajkumar, et al., International myeloma working group consensus recommendations on imaging in monoclonal plasma cell disorders, *Lancet Oncol.* 20 (2019) e302–e312, [https://doi.org/10.1016/S1470-2045\(19\)30309-2](https://doi.org/10.1016/S1470-2045(19)30309-2).
- [8] A.J. Cowan, D.J. Green, M. Kwok, et al., Diagnosis and Management of Multiple Myeloma: A Review, *J. Am. Med. Assoc.* 327 (2022) 464–477, <https://doi.org/10.1001/jama.2022.0003>.
- [9] A.G. Ormond Filho, B.C. Carneiro, D. Pastore, et al., Whole-Body Imaging of Multiple Myeloma: Diagnostic Criteria, *Radiographics* 39 (2019) 1077–1097, <https://doi.org/10.1148/rg.2019180096>.
- [10] S.V. Rajkumar, M.A. Dimopoulos, A. Palumbo, et al., International Myeloma Working Group updated criteria for the diagnosis of multiple myeloma, *Lancet Oncol.* 15 (2014) e538–e548, [https://doi.org/10.1016/S1470-2045\(14\)70442-5](https://doi.org/10.1016/S1470-2045(14)70442-5).
- [11] S.V. Rajkumar, Multiple myeloma: 2022 update on diagnosis, risk stratification, and management, *Am. J. Hematol.* 97 (2022) 1086–1107, <https://doi.org/10.1002/ajh.26590>.
- [12] D. Ippolito, C.T. Franzesi, S. Spiga, et al., Diagnostic value of whole-body ultra-low dose computed tomography in comparison with spinal magnetic resonance imaging in the assessment of disease in multiple myeloma, *Br. J. Haematol.* 177 (2017) 395–403, <https://doi.org/10.1111/bjh.14545>.
- [13] E. Zamagni, M. Cavo, The role of imaging techniques in the management of multiple myeloma, *Br. J. Haematol.* 159 (2012) 499–513, <https://doi.org/10.1111/bjh.12007>.
- [14] C. Thomas, C. Schabel, B. Krauss, et al., Dual-Energy CT: Virtual Calcium Subtraction for Assessment of Bone Marrow Involvement of the Spine in Multiple Myeloma, *Am. J. Roentgenol.* 204 (2015) W324–W331, <https://doi.org/10.2214/AJR.14.12613>.
- [15] A. Kosmala, A.M. Weng, A. Heidemeier, et al., Multiple Myeloma and Dual-Energy CT: Diagnostic Accuracy of Virtual Noncalcium Technique for Detection of Bone Marrow Infiltration of the Spine and Pelvis, *Radiology* 286 (2018) 205–213, <https://doi.org/10.1148/radiol.2017170281>.
- [16] A. Kosmala, A.M. Weng, B. Krauss, S. Knop, T.A. Bley, B. Petritsch, Dual-energy CT of the bone marrow in multiple myeloma: diagnostic accuracy for quantitative differentiation of infiltration patterns, *Eur. Radiol.* 28 (2018) 5083–5090, <https://doi.org/10.1007/s00330-018-5537-5>.
- [17] P. Fervers, F. Fervers, J. Kottlors, et al., Feasibility of artificial intelligence-supported assessment of bone marrow infiltration using dual-energy computed tomography in patients with evidence of monoclonal protein - a retrospective observational study, *Eur. Radiol.* 32 (2022) 2901–2911, <https://doi.org/10.1007/s00330-021-08419-2>.
- [18] C. Hu, Y. Zhang, X. Xiong, et al., Quantitative evaluation of bone marrow infiltration using dual-energy spectral computed tomography in patients with multiple myeloma, *J. Xray Sci. Technol.* 29 (2021) 463–475, <https://doi.org/10.3233/XST-200811>.
- [19] M.T. Tan, T.B. Lloyd, Utility of dual energy computed tomography in the evaluation of infiltrative skeletal lesions and metastasis: a literature review, *Skeletal Radiol.* 51 (2022) 1731–1741, <https://doi.org/10.1007/s00256-022-04032-6>.
- [20] G. Schröder, M. Reichel, S. Spiegel, et al., Breaking strength and bone microarchitecture in osteoporosis: a biomechanical approximation based on load tests in 104 human vertebrae from the cervical, thoracic, and lumbar spines of 13 body donors, *J. Orthop. Surg. Res.* 17 (2022) 228, <https://doi.org/10.1186/s13018-022-03105-5>.
- [21] C.P. Reinert, E. Krieg, M. Esser, K. Nikolaou, H. Bösmüller, M. Horgner, Role of computed tomography texture analysis using dual-energy-based bone marrow imaging for multiple myeloma characterization: comparison with histology and established serologic parameters, *Eur. Radiol.* 31 (2021) 2357–2367.
- [22] M. Li, L. Zhang, W. Tang, Y.J. Jin, L.L. Qi, N. Wu, Identification of epidermal growth factor receptor mutations in pulmonary adenocarcinoma using dual-energy spectral computed tomography, *Eur. Radiol.* 29 (6) (2019) 2989–2997, <https://doi.org/10.1007/s00330-020-07320-8>.
- [23] H. Michael, L. Tian, M. Ghebremichael, The ROC curve for regularly measured longitudinal biomarkers, *Biostatistics* 20 (3) (2019) 433–451, <https://doi.org/10.1093/biostatistics/kxy010>.
- [24] I. Telias, D. Junhasavasdikul, N. Rittayamai, et al., Airway Occlusion Pressure as an Estimate of Respiratory Drive and Inspiratory Effort during Assisted Ventilation, *Am. J. Respir. Crit. Care Med.* 201 (9) (2020) 1086–1098, <https://doi.org/10.1164/rccm.201907-1425OC>.
- [25] D. Rades, E.M. Werner, E. Glatzel, et al., Early Identification of Pneumonitis in Patients Irradiated for Lung Cancer-Final Results of the PARALUC Trial, *Cancers (basel)* 15 (2) (2023) 326, <https://doi.org/10.3390/cancers15020326>.
- [26] S.V. Rajkumar, M.A. Dimopoulos, A. Palumbo, et al., International Myeloma Working Group updated criteria for the diagnosis of multiple myeloma, *Lancet Oncol.* 15 (12) (2014) e538–e548, [https://doi.org/10.1016/S1470-2045\(14\)70442-5](https://doi.org/10.1016/S1470-2045(14)70442-5).
- [27] S.V. Rajkumar, Multiple myeloma: 2024 update on diagnosis, risk-stratification, and management, *Am. J. Hematol.* 99 (9) (2024) 1802–1824, <https://doi.org/10.1002/ajh.27422>.
- [28] M.A. Dimopoulos, J. Hillengass, S. Usmani, et al., Role of magnetic resonance imaging in the management of patients with multiple myeloma: a consensus statement, *J. Clin. Oncol.* 33 (6) (2015) 657–664, <https://doi.org/10.1200/JCO.2014.57.9961>.
- [29] J. Chen, Z. Qiu, N. Jiang, et al., Detecting bone marrow infiltration in nonosteolytic multiple myeloma through separation of hydroxyapatite via the two-material decomposition technique in spectral computed tomography, *Quant. Imaging Med. Surg.* 14 (3) (2024) 2345–2356, <https://doi.org/10.21037/qims-23-1042>.
- [30] G. Cherya, S. Sharma, A. Chhabra, Dual energy CT in musculoskeletal applications beyond crystal imaging: bone marrow maps and metal artifact reduction, *Skeletal Radiol.* 51 (2022) 1521–1534, <https://doi.org/10.1007/s00256-021-03979-2>.